

Bone Segmentation in CT-Liver images using K-Means Clustering for 3D Rib Cage Surface-Modeling

Walita NARKBUAKAEW¹, Hiroshi NAGAHASHI², Kota AOKI², Yoshiki KUBOTA³

¹Interdisciplinary Graduate School of Science and Engineering

Tokyo Institute of Technology, Kanagawa, Japan

²Imaging Science and Engineering Laboratory

Tokyo Institute of Technology, Kanagawa, Japan

³Gunma University Heavy-Ion Medical Center, Gunma, Japan

narkbuakaew.w.aa@m.titech.ac.jp, longb@isl.titech.ac.jp,

aoki.k.af@m.titech.ac.jp, and y_kubota@gunma-u.ac.jp

Abstract: A 3D rib cage model helps to study anatomical structures in some medical applications such as biomechanical and surgical operations. Its quality directly depends on rib cage segmentation if it is reconstructed from image data. This paper presents an optional segmentation method based on K-means clustering. It uses a hierarchical concept to control the clustering, and it organizes clustered regions in subsequent indexes of background, soft-tissue, and hard-tissue regions. We applied the proposed method to 3D CT-liver images acquired by a 4D-CT imaging system. The proposed method was compared with 2D K-means (KM) and 2D fuzzy C-means (FCM) clustering. From our experiment, the proposed method gave more stable clustering results under a condition of randomization in initial cluster-centers, and it performed faster than 1.5 times of 2D-KM and 7.7 times of 2D-FCM on average. For 3D surface models, the results of the proposed method provided more information of bone regions in vertebra, ribs, and scapula areas than results of 2D-KM and 2D-FCM.

Key-Words: 2D K-mean clustering, 2D fuzzy C-mean clustering, and rib cage segmentation

1 Introduction

Rib cage [1] is a fundamental structure that protects heart and lungs, and it supports respiration. It is formed by sternum and costal cartilages, vertebral column, and ribs. In addition, a 3D model of the rib cage probably assists in studying scoliosis, biomechanics, and surgical operation [2, 3, 4].

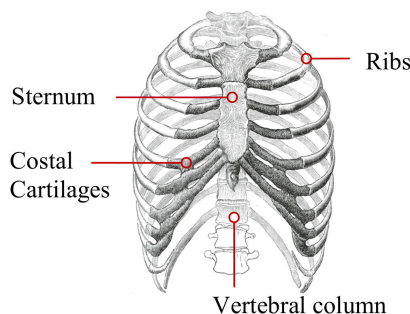


Fig. 1: An anterior view of rib cage structure [5]

Furthermore, medical image segmentation is a fundamental process of computer-aided diagnosis (CAD), computer assisted surgery (CAS), and 3D visualization. Many algorithms are continuously pro-

posed to handle specific problems. For example, thresholding [6] was used to segment long bones from computed tomography (CT) data. A 3D model can be reconstructed from this segmentation result to support implant design, finite element analysis, and computer-aided surgical planning. A region growing technique [7] including some knowledge constraints was employed to segment liver-tumor in contrast-enhanced CT data. Knee bone structures were extracted by an active contour method [8] for constructing the 3D model. A kind of these methods performs well when edge or region information of a target organ is demonstrated separately from neighbors in a given image. Further, they sometimes require prior knowledge to produce a training data set. Additionally, an image segmentation approach based on clustering is one of interesting methods. The clustering is an unsupervised method that simultaneously separates data points into several groups. Therefore, we do not need a training data set. Further, it supports feature vectors containing multiple components. These kinds of methods have been developed in a wide range of research areas [9, 10]. Generally, in the process of image segmentation, each pixel is represented as a

feature vector containing one or many components. These components can be selected from the possible features of geometry, texture, and gradient [11, 12]. Then, the pixel is clustered into an appropriate group through an objective function that is designed to measure a distance or a similarity. For instance, Mignotte M. [13] applied K-means clustering algorithm to different color channels and integrated the results in the segmentation of natural images. Lee, T.H. et al. [14] used K-means clustering to segment normal and abnormal regions in CT brain images. Then, a decision tree based on six features was constructed to classify the abnormal regions. Further, they used an expectation-maximization (EM) algorithm to extract cerebrospinal fluid (CSF) and brain matter. Juang, L.H. et al. [15] introduced a tumor tracking method by applying K-means clustering to the MRI brain images in converted color-spaces. Yusoff I.A. et al. [16] proposed an image segmentation method base on two-dimensional clustering for natural-and cervical cells images. Then, they introduced a method to determine the number of clusters in [17]. Selvy P.T. et al. [18] examined MRI brain image segmentation to detect Cerebrospinal Fluid (CSF). They combined anisotropic diffusion and total variation regularization with Fuzzy C-Means to handle image noise. Then, they [19] applied a particle swarm optimization to achieve a global optimal solution. Chu et al. [20] used a clustering method to divide an atlas database for acquiring the best matching between a given image and a template image. Next, they constructed a dynamic weight function and used maximum a posterior probability (MAP) estimation to perform multi-organ segmentation. Actually, many studies presented their attractive results under particular features and extension of an objective function that possibly causes complexity of computation. Further, most of these studies did not mention about indexing that is necessary to identify some parts of all clustering regions. Therefore, we are motivated to use the clustering method for rib cage segmentation, which directly influences quality of 3D surface reconstruction.

Indeed, we attempt to develop a segmentation method under simple conditions to achieve a good quality of 3D rib cage model. This paper presents a 2D K-means clustering method including a hierarchical concept and cluster indexing. We apply the proposed method to 10 sets of 3D CT-liver images, which were acquired by a 4D-CT imaging system. Then, the proposed method is compared with 2D K-Means and 2D Fuzzy C-Means clustering by investigating different points in clustered regions, stability in results of clustering, and computation time.

The rest of this paper is organized as follows. Section 2 briefly describes concepts of related meth-

ods. Then, we explain the proposed method in section 3. Next, section 4 shows experimental results. Lastly, we summarize this study in section 5.

2 Related Method

2.1 K-means clustering (KM)

The K-mean clustering [21] is normally introduced to divide data points $X = \{x_1, \dots, x_N\}$ into K clusters. It supports multi-dimensional vectors and gives high efficiency of computation. The purpose of this algorithm is to minimize the objective function of

$$J_{\text{KM}} = \sum_{n=1}^N \sum_{k=1}^K b_{nk} \|x_n - c_k\|^2, \quad (1)$$

$$b_{nk} = \begin{cases} 1 & \text{if } k = \arg \min_a \|x_n - c_a\|^2, a = 1, \dots, K, \\ 0 & \text{otherwise,} \end{cases}$$

$$c_k = \frac{1}{N_k} \sum_{x \in C_k} x,$$

where $\|\cdot\|$ is a distance measure. The variables c_k and N_k denote the center and the number of data points in the cluster C_k . This algorithm can be summarized as follows.

Step 1: Initialize the cluster centers $\{c_1, \dots, c_K\}$ by randomly sampling the data points from X .

Step 2: Measure distances among all data points and all cluster centers.

Step 3: Label cluster index (k) to each data point by considering the shortest distance.

Step 4: Determine new clusters centers from all member points in the same cluster.

Step 5: Repeat step 2 to 4 until the cluster labels do not change.

2.2 Fuzzy C-means (FCM)

The fuzzy C-means clustering [22] describes each data point through a degree of memberships in all clusters C instead of a binary clustering as K-means clustering. If data is $X = \{x_1, \dots, x_N\}$, the objective function to be minimized is

$$J_{\text{FCM}} = \sum_{n=1}^N \sum_{j=1}^C (u_{nj})^m \|x_n - c_j\|^2, \quad (2)$$

$$u_{nj} = \frac{1}{\sum_{k=1}^C \left(\frac{\|x_n - c_k\|}{\|x_n - c_j\|} \right)^{\frac{2}{m-1}}},$$

$$c_j = \frac{\sum_{n=1}^N u_{nj}^m \cdot x_n}{\sum_{n=1}^N u_{nj}^m},$$

where u_{nj} is a degree of membership, and c_j is the cluster center. The variable $m \geq 1$ is a weight exponent, and its default parameter is equal to two. Similarly, we can minimize the objective function of the FCM clustering by using an iteration procedure.

Step 1: Initialize a matrix of membership $U^{(t=0)} = \{u_{nj}\}$ through randomization where t is an index of iteration.

Step 2: Calculate the cluster center c_j

Step 3: Measure distances among all data points and all clusters centers.

Step 4: Update a degree of membership $U^{(t+1)}$

Step 5: Compare $\|U^{(t+1)} - U^t\| < \varepsilon$, where ε is a constant that is used to stop the iteration. Otherwise, return to step 2.

2.3 Two-dimensional K-means (2D-KM)

Yusoff I.A. et al. [16] defined each feature vector including two components to represent each pixel in the image. One component is gray intensity and the other is median intensity that is obtained from applying a 3x3 median filter. This method was applied to some natural and cervical-cell images. In their experiment, the use of K-means clustering with two feature components gave the better segmentation results than the use of only gray intensity in K-means, Fuzzy C-means, and moving K-means clustering [23].

However, although the results of Yusoff I.A. et al [16] showed some improvement in 8-bits image, it may not perform well in 16-bits CT-liver images that include high levels of image noise and some artifacts. Moreover, they did not consider labeling in the clustering results. Thus, if we have many images and we randomly initialize cluster centers, it is impractical to select a clustered region giving a desirable type of tissue through an index of the cluster center because cluster labels are normally random.

3 Proposed Method

This study proposes some specific conditions to improve bone segmentation in CT-liver images based on K-means clustering. We produce the proposed method from two main ideas.

First, gray intensities inside CT images are described by CT numbers in the Hounsfield unit (HU) that is computed from the linear attenuation coefficients of tissues [24, 25]. The attenuation coefficient of water is a reference. If material attenuates more than water, a CT number will be positive. Otherwise, it presents a negative CT number when its attenuation is less than water. Therefore, no hard tissue regions are expressed by an intensity range of soft tissues. For

instance, CT numbers of air, muscle, and bone are -1000, 10, 1000 HU, respectively. Second, we should remove undesirable information to reduce complexity in clustering, and a binary-hierarchical concept helps to achieve this assumption for CT-liver images. For example, from a global point of view, a given image contains air (background) and a patient's body (foreground) regions. Next, information inside the body region consists of soft-and hard-tissue regions. Therefore, we should remove information of air before performing a new clustering process to separate soft and hard tissue regions.

The proposed method (See Fig. 2) begins with feature extraction to acquire statistical feature description of each pixel. Next, we apply K-means clustering to feature vectors for dividing them into two clustered regions. Then, we give simple conditions to identify which one should be an object region. Afterwards, we check some conditions to terminate the segmentation process. We stop the segmentation process when proportions of differences in size and gray intensities between two regions are small. Thus, if the stop conditions are verified, we should merge both regions, and integrate them into a final clustering result. Otherwise, if the stop conditions are not satisfied, we will repeat clustering on feature vectors inside the object region. Further, the other region called a background is combined to the final clustering result. Finally, we identify the final clustered regions by giving subsequent indexes of background, soft-tissues and hard-tissue regions.

3.1 Feature extraction

In this study, we explain a feature vector as a data point that is mapped onto a feature space. Each component in one feature vector presents a coordinate in one axis. Thus, for example, if a given image contains N pixels and one feature consists of M components, we will get a set of feature-vectors \mathcal{F} including N vectors, which are located in a M -dimensional clustering-space. We can explain this definition by

$$\mathcal{F} = \{\mathbf{f}(i) \mid 1 \leq i \leq N\}, \quad (3)$$

$$\mathbf{f}(i) = \{v(i, m) \mid 1 \leq m \leq M\},$$

where $\mathbf{f}(i)$ denotes a feature vector and $v(i, m)$ is a feature component of the vector $\mathbf{f}(i)$. The index of feature vector is $i = x + (y \times \text{width of image})$ and $i = x + (y \times \text{width of image} \times \text{height of image})$ in 2D and 3D discrete-space coordinate systems, respectively. In this study, we use two methods to extract features:

a) Directly use gray intensity in each pixel x of a given image $v(i, m) = I(x)$, where $x = (x, y)$ in 2D and $x = (x, y, z)$ in 3D image data.

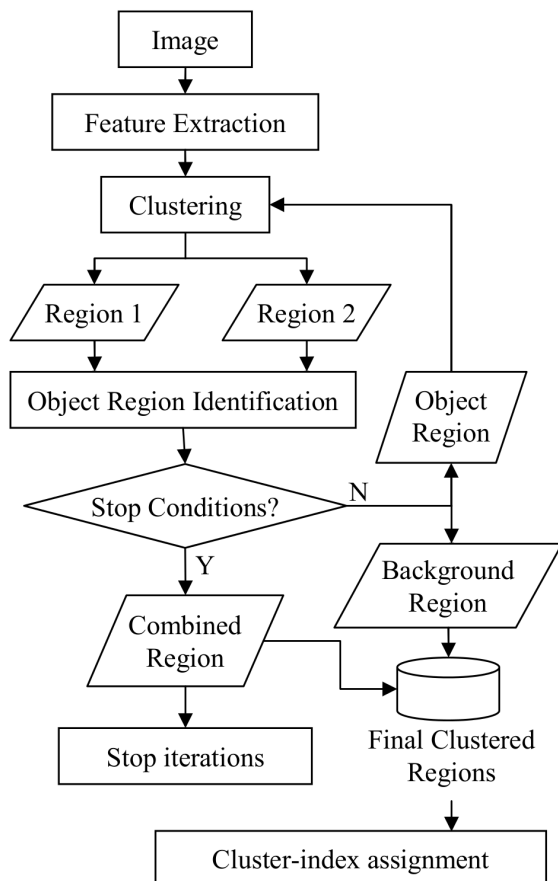


Fig. 2: A diagram of a proposed procedure for CT image-segmentation

b) Apply a filter (F) to a given image, and then gray intensity value in each pixel represents a feature component $v(i, m) = I_F(x)$, where I_F is a filtered image.

3.2 Definition of cluster centers

We describe cluster centers in the form of a coordinate system of feature components as

$$c_k(m_1, \dots, m_M) = \frac{1}{N_k} \left(\sum_{p \in C_k} v(p, 1), \dots, \sum_{p \in C_k} v(p, M) \right), \quad (4)$$

where $v(p, 1)$ and $v(p, M)$ are the first and the last components of a feature vector that is a member of cluster C_k and indexed by p . The variable N_k denotes the total number of feature vectors in the cluster C_k . Therefore, a mean value of each component in the same cluster C_k represents a position of the cluster center in each axis of the clustering space.

3.3 Object-region identification and stop conditions

After feature vectors are clustered into two groups by the K-mean clustering, we generate a region r_k (or volume in 3D data) for each group by backward transforming indexes of feature vectors to the domain of a given image and using the following condition.

$$r_k(x) = \begin{cases} 1 & \text{if } f(i) \in C_k, k = 1, 2, \\ 0 & \text{otherwise.} \end{cases} \quad (5)$$

Next, we need means of gray intensities μ_1 and μ_2 to refer to the CT numbers of the both clustered regions. Thus, these mean values approximately demonstrate types of materials in the CT images. For example, if μ_k is a negative value, the clustered region is equivalent to air. However, each clustered region r_k is described as a binary image. Therefore, in order to determine the mean of gray intensities inside the clustered region r_k , we require a remapping function $\mathcal{R}(\cdot)$ to remap gray intensities from a given image as

$$\mathcal{R}(r_k, I) = r_k(x) \cdot I(x). \quad (6)$$

Furthermore, we use a threshold T_{gray} to limit a range of intensities in the same type of materials or tissues. Then, the sums of clustered members in the both clustered regions (s_1 and s_2) are obtained, and we use a threshold T_{size} to define size of the small group that should not be further clustered in the next iteration.

From parameters r_k , μ_k , s_k , T_{gray} , and T_{size} , we can produce conditions to identify the object region r_{obj} and background region r_{bkg} , and to stop iterations of the binary-hierarchical clustering as shown in Algorithm 1. In summary, we give three ideas to generate this algorithm. First, the difference in means of gray intensities between two clustered regions should be large adequately to verify that both clustered regions are not the same type of materials or tissues. Second, it is not necessary to further divide a region possibly including one type of material or a small region into two particle regions. Third, the region giving a higher mean of gray intensities is possible to be the object region more than the background region if its size is large adequately.

3.4 Cluster-indexing

Normally, the result of K-means clustering illustrates a set of cluster labels in according with the indexes of cluster centers. However, if we randomly initialize cluster centers, the same index of cluster center will not be moved to the same position in every time of testing. Thus, the labels of the clustered regions will be different. For example, a background region in the

Algorithm 1 Object-region identification and stop conditions

Input: $r_1, r_2, \mu_1, \mu_2, s_1, s_2, T_{\text{gray}}$ and T_{size}
Output: $r_{\text{obj}}, r_{\text{bkg}}$, flag of stop iteration
If $|\mu_1 - \mu_2| > T_{\text{gray}}$ or $(s_1 + s_2) > T_{\text{size}}$
If $\mu_1 > \mu_2$
 If $s_1 > T_{\text{size}}$ and $s_2 > 0$
 $r_{\text{obj}} = r_1$ and $r_{\text{bkg}} = r_2$
 Else If $s_2 > T_{\text{size}}$ and $s_1 > 0$
 $r_{\text{obj}} = r_2$ and $r_{\text{bkg}} = r_1$
 Else stop iteration = true and $r_{\text{bkg}} = r_1 \cup r_2$
 End If
Else
 If $s_2 > T_{\text{size}}$ and $s_1 > 0$
 $r_{\text{obj}} = r_2$ and $r_{\text{bkg}} = r_1$
 Else If $s_1 > T_{\text{size}}$ and $s_2 > 0$
 $r_{\text{obj}} = r_1$ and $r_{\text{bkg}} = r_2$
 Else stop iteration = true and $r_{\text{bkg}} = r_1 \cup r_2$
 End If
End If
Else
 stop iteration = true and $r_{\text{bkg}} = r_1 \cup r_2$
End If

first time of testing is labeled by one, but this background region may be labeled by two in the second time of testing. Thus, it is difficult to access a desirable region through an index of a cluster center. This problem is simply solved by using a mean of gray intensities inside a region for deciding its label. However, this solution fails when we consider more than one data set. Since, each material or tissue in CT images is represented by a range of gray intensities and some data sets are forced by some artifacts or image noises. The means of gray intensities inside the same type of tissue in different data sets occasionally present different values.

Consequently, we propose a simple method to solve this problem. It starts from remapping gray intensities into each clustered region by using (6). Next, we calculate mean value μ_k of all remapping regions, and then we obtain cluster index T by comparing with a set of possible means of gray intensities in different clusters, e.g. $P = \{-1000, 0, 50, 200\} \approx \{\text{background}, \text{soft-tissue1}, \text{soft-tissue2}, \text{hard-tissue}\}$. These values are designed and adjusted by considering average intensities of standard CT numbers in each type of tissues. The cluster indexing is defined by

$$T = \arg \min_t |P(t) - \mu_k|. \quad (7)$$

Consequently, this method helps to organize the clustered regions into subsequent indexes of background,

soft-tissue, and hard-tissue regions.

3.5 3D Rib cage surface modeling

We extensively use the 2D-KM, 2D-FCM, and the proposed clustering method to segment the rib cage in a 3D-CT data set. Thus, each voxel corresponds to a feature vector. Then, we evaluated quality of rib cage segmentation by comparing completeness of 3D surface models in different viewpoints. Since, in our data set, accurate ground truth of rib cage segmentation is not available and manual labeling is a time consuming process.

In order to construct a 3D surface model, we start from selecting bone regions in the clustering results. We manually choose the index of bone regions inside the clustering results of 2D-KM and 2D-FCM. Meanwhile, the clustering results of the proposed method is demonstrated by subsequent indexes of background, soft-tissue and hard-tissue regions. Thus, we select hard-tissue regions to represent bone regions.

Next, we apply a 5x5 median filter to each axial-image plane in the 3D segmented data. We use this filter to reduce particle regions, which are diffusely appeared due to high level of image noises and some artifacts. Afterwards, a surface model is reconstructed by the Marching cubes [26] algorithm.

4 Experiment and Results

4.1 Data set

We applied the proposed method to 3D CT images of ten respiratory phases (i.e. 10 sets of 3D CT data) of a 4D CT-liver data set. This data is collected from a patient by using a GE Discovery ST and a Varian RPM system in a cine mode. Further, it is provided by the MIDAS community, <http://midas.kitware.com/community/view/47>. Each 3D CT data set contains 150 slices of 16-bits axial image slices. A size of each axial image slice is 512x512 pixels with resolution 0.98 square millimeters, and slice thickness is 2.5 millimeters. Further, we assigned the region of interest (ROI) to neglect computation in unnecessary regions allocated outside the patient's body in each axial image. The ROI covers an area from a top-left coordinate (30,70) to a bottom-right coordinate (495,380); therefore, the remaining data in each axial-image sizes 466x311 pixels.

4.2 2D-CT multiple-region segmentation

In this section, we randomly sampled 10 images from a 3D-CT data set to investigate some properties of the proposed clustering method. The slice indexes of them were 14, 19, 41, 82, 94, 122, 135, 137, 140, and

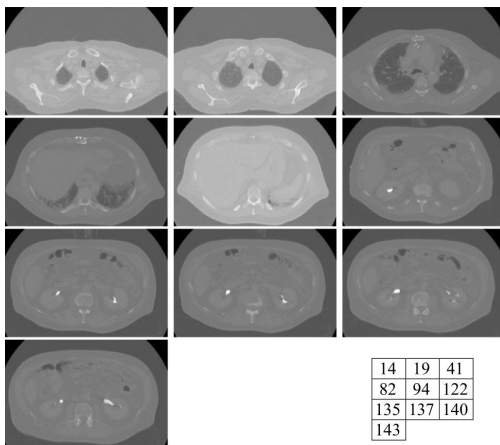


Fig. 3: Ten examples of original axial images

143 (see Fig. 3). Moreover, for the proposed method, we assigned $T_{\text{size}} = 10\%$ of the total image size, and $T_{\text{gray}} = 20$, and applied these parameters to all experiments. We obtained these thresholds from manually adjustment through applying the proposed method to an sample axial image.

4.2.1 Stability in results of clustering

Normally, initial cluster-centers from randomization can cause different clustering results in both clustered regions and labels (See Fig. 4). It is simply solved by repeating the clustering processes until a desirable result is released. However, it is a time-consuming process when a given image contains a large number of feature vectors and a target region is a small region. Therefore, this condition causes clustering results to be unstable. Consequently, we investigated the influence of random cluster-centers on the proposed clustering method.

We randomly initialized cluster-centers and created two feature components from gray intensity and median gray value that was produced by applying a 3×3 median filter. We tested 100 times for each sample axial-images. Then, we observed the number of different clustering results. The small number of differences in clustering-results represents high stability. Further, we considered a proportion of bone-region appearance in the clustered results in order to recheck possibility of rib cage segmentation. The results of the proposed method were compared with the results of 2D-KM and 2D-FCM clustering methods. In this comparison, we applied the same feature components and the results were shown on Table 1.

From Table 1, the proposed method showed the most stability in clustering results when a number of clusters in 2D-KM and 2D-FCM were equal to four, five, and six clusters. Furthermore, it was able to illus-

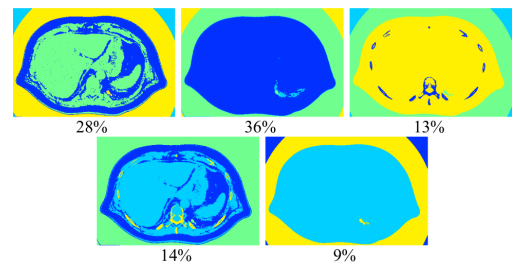


Fig. 4: Five examples of 2D-KM clustering results at CT axial image slice 94 when initial cluster-centers are random, the number of clusters is four and feature components are gray intensity and median gray (results of convolution between 3×3 median filtering and a given image); the percentage presents the number of images that give the same regions from 100 times of testing.

trate bone region in all results of clustering although clustered regions were different (see Fig. 6 (a) and (b)). Otherwise, it was possible to increase a possibility of bone-region appearance in the results of 2D-KM and 2D-FCM clustering by adding the number of clusters. However, the increase of the number of clusters caused stability of clustering to drop because the number of different clustering results was raised up. Moreover, it gradually improved the possibility of bone-region appearance in some images as shown in Fig. 5.

In addition, although the proposed method presented higher stability in results of clustering, it is occasionally better to get only one type of clustering results if we consider multiple organs [27]. We achieved this requirement by giving a simple condition (called a mean-group) on the initial cluster centers. We symmetrically divide feature vectors into two sections for every use of the proposed clustering method. Then, we select mean value of each section to represent an initial cluster-center.

$$c_k = (m_x^k, m_y^k), \quad k = 1, 2 \quad (8)$$

$$\begin{aligned} m_x^k &= \text{Mean} \left(\{v(i, 1)\}_{i=D_0}^{D_1} \right), \\ m_y^k &= \text{Mean} \left(\{v(i, 2)\}_{i=D_0}^{D_1} \right), \\ D_0 &= \frac{N \times (k - 1)}{2} + 1, \quad D_1 = \frac{N \times k}{2} \end{aligned}$$

where c_k is cluster center indexed by k . The variable N denotes the number of feature vectors. Further, this condition did not change the final clustering results as shown in Fig. 6 (c).

Table 1: Influence of the random cluster-centers in initialization; it tests on 10 sample images and 100 times in each image. Assign 4, 5, and 6 clusters to 2D-KM (A) and 2D-FCM (B) whereas the proposed clustering without (C) and with (D) indexing (7) use $P = \{-1000, 0, 50, 200\}$;

Description of measures	Clustering Methods							
	K = 4		K = 5		K = 6		C	D
	A	B	A	B	A	B		
The maximum number of different clustering-results	5	2	6	3	4	5	3	2
The average number of different clustering-results	3.9	1.2	4.3	2.1	3.9	2.0	2.1	1.6
The average percentage of bone-region appearances	19.7	0.0	25.1	8.6	36.2	65.9	100	100

(Note: K denotes the number of clusters)

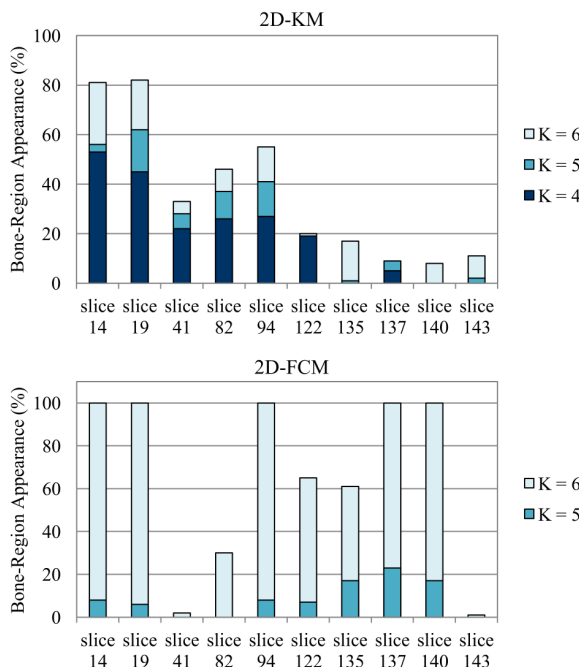


Fig. 5: Two bar charts of percentages of bone-region appearances in clustering results of 2D-KM (top) and 2D-FCM (bottom) when the number of clusters is increased.

4.2.2 Compare 2D multiple-region segmentation

In this section, we defined gray intensities and median gray values as feature components, which were used in the proposed clustering method, 2D-KM, and 2D-FCM. We set the number of clusters to be six for applying to 2D-KM and 2D-FCM. Meanwhile, we initialized two possible sets of means of gray intensities in different clusters (referred to (7)) to study an effect of them. They were $P_1 = \{-1000, 0, 50, 200\}$ and $P_2 = \{-1000, 0, 40, 80, 150, 300\}$. These sets produced two maximum number of clusters, which were four and six clusters, respectively. For initial cluster-centers, we randomized feature vectors to represent cluster-centers in 2D-KM and 2D-FCM. Otherwise,

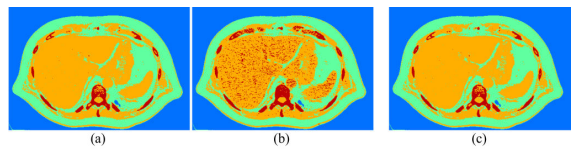


Fig. 6: An examples of two different clustering- results (a) and (b) at CT-axial image slice 94 performed by the proposed clustering method with $P_1 = \{-1000, 0, 50, 200\}$ when initial cluster centers are random. (c) presents an example result when initial cluster-centers depend on mean value.

we used a mean group condition (8) to initialize cluster centers for the proposed method. We performed 2D-KM and 2D-FCM for 10 times to obtain the best results of them before comparing with the proposed method. Several examples of clustering results were demonstrated in Fig. 7.

First, we considered air regions allocated outside a patient's body and inside lungs. The proposed method gave only one label (see arrows at the top of images in the first rows and arrows in the second row). Meanwhile, 2D-KM and 2D-FCM presented three different labels in these areas. This difference appears because both 2D-KM and 2D-FCM does not consider type of materials. Further, the air regions allocated outside the patient's body in CT-liver images normally displays two levels of gray intensities because of some artifacts (see Fig. 3).

Next, the proposed method possibly enhanced boundaries of vertebra regions as shown in enlarged images (Fig. 8) of the first and third rows in Fig. 7. Actually, we found some boundaries of vertebra regions in the results of 2D-KM and 2D-FCM were lost.

Further, the set of mean-intensities (P_1 or P_2) assisted to separate regions including small different gray levels. For example, the result of the proposed method with P_2 in the last row of Fig. 7. Some parts of the kidney regions were separated from bone regions and another soft-tissue whereas comparatives

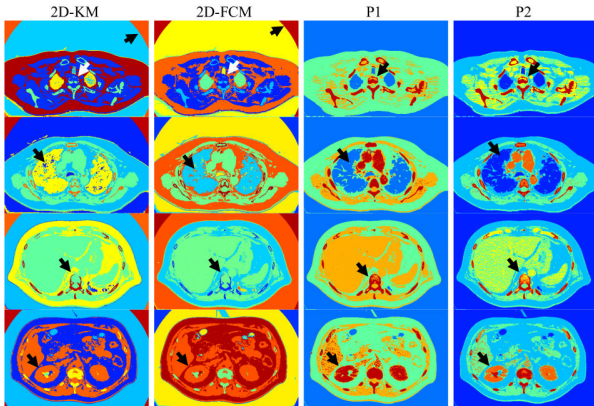


Fig. 7: Four comparisons of example results of four different clustering methods in axial slices 14, 41, 94, and 122 from top-to-bottom rows; these methods are 2D-KM, 2D-FCM, the proposed method with $P_1 = \{-1000, 0, 50, 200\}$ and $P_2 = \{-1000, 0, 40, 80, 150, 300\}$ in left-to-right order.

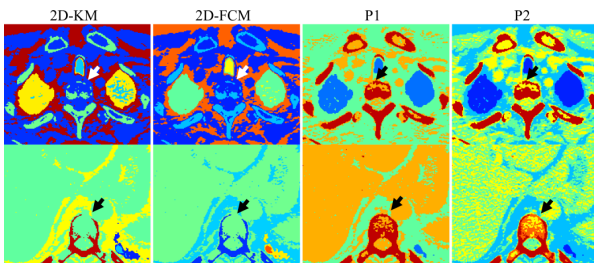


Fig. 8: Two examples of bone-region enhancement displayed through enlarged images of the 1st and 3rd rows in Fig. 7.

methods failed to distinguish them. However, if this set includes many levels of means of gray intensities, the problem of noise or particle regions will be appeared.

4.3 Compare 3D rib cage model

From 10 sets of 3D-CT data, we almost performed three times of testing on 2D-KM and 2D-FCM to select the best clustering results for each set of 3D-CT data. Occasionally, we further computed more than three times when no clustering results presented bone regions. Otherwise, although the proposed method did not require replication of a clustering process, we repeatedly computed it three times to obtain average of computation time and compared with 2D-KM and 2D-FCM methods. We found the proposed method spent 103 seconds to segment multi-regions in a 3D-CT data set on average. Meanwhile, 2D-KM and 2D-FCM required about 157 and 794 seconds. These computations were performed under the MATLAB

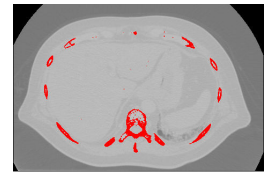


Fig. 9: An example of manual threshold adjustment (216,1235) at an axial image slice 94

environment on 3.40 GHz Intel(R) Core(TM) i7-2600 CPU.

Next, we examined quality of rib cage surface models. We observed eight points labeled by (A) to (H) labels (see Fig 10). We used color shade to explain the depth of model from front to back, and this shade helped to observe ribs. This investigation further included the result of manual threshold that was adjusted through considering threshold labels at an axial image slice 94 as shown in Fig. 9. Then, we applied this threshold to a whole 3D-CT data set for getting a rib cage segmented volume.

From our experiment, 3D rib cage surface models, which were reconstructed from segmentation results of manual threshold, 2D-KM, 2D-FCM, and the proposed method, demonstrated some different viewpoints.

First, the bone regions in the top area of the model were labeled by (A). We did not find the lost regions in the results of manual threshold and the proposed method. Second, large areas of rib bones in the front (B) and bottom (F) views disappeared in the results of 2D-KM and 2D-FCM. Otherwise, the results of manual threshold and the proposed method gave more details but they were unable to illustrate costal cartilages. Further, in the results of manual threshold and the proposed method, they presented clear boundaries of ribs in the bottom area of the side (G) and back (E) views. Next, only the results of the proposed method showed regions of scapular bones (D) without losing the large areas. Subsequently, we considered spine regions (H). The results of 2D-KM, 2D-FCM presented lost regions around anterior areas of vertebrae in many sections of spine. The results of manual threshold illustrated small lost regions around anterior areas of vertebrae in the top and bottom sections of spine. These lost regions were possibly found because we adjusted threshold on the sample image allocated around the center of a 3D-CT data set and this data set includes large variation in gray intensities among different axial-image planes due to some artifacts. The results of the proposed method did not show the lost regions around anterior areas of vertebrae, but small regions of vertebrae in the top section of spine were merged. Lastly, the results of the proposed method

presented large areas of kidneys that were undesirable regions. However, these kidney volumes separated from bone regions. Thus, it is not difficult to remove them. Otherwise, the results of manual threshold, 2D-KM, and 2D-FCM displayed them in small areas.

5 Conclusion

This paper introduces an optional segmentation method based on a K-mean clustering algorithm. It is aimed to enhance bone-segmented regions in CT-liver images under high levels of image noise and some artifacts. The proposed method contains two main conditions. First, we used a hierarchical concept to manage feature vectors and clustering regions. We produced a simple algorithm to identify type of clustering region and control iteration. Thus, we do not want to define the total number of clusters before starting the process. Second, we created a cluster indexing method to control labels of clustered regions in the clustering results. Further, this indexing relates to types of tissues or CT standard numbers by representing subsequent indexes of background, soft tissue, and hard tissue regions.

We applied the proposed method to 10 sets of 3D CT data, and the results were compared with 2D-KM and 2D-FCM methods. From comparison, the proposed method gave more stable results when initial cluster centers were random. A percentage of bone-region appearances in the clustering results of the proposed method was higher than 2D-KM and 2D-FCM. Further, boundary information of bone-regions were illustrated more than two comparative methods. We observed eight points allocated in different locations of 3D surface models to investigate different results. In summary, the segmentation results of the proposed method seemed to give more information of bone regions in vertebra, ribs, and scapula areas than the results of 2D-KM and 2D-FCM. Conversely, the proposed method cannot prevent appearance of large kidney-regions in the segmentation results. In addition, the proposed method required computation time less than 2D-KM and 2D-FCM for 1.5 and 7.7 times of computation in one 3D-CT data on average.

However, the proposed method requires manual adjustment on several parameters. Further, the clustering relied on the basic feature components, gray and median gray, that cannot completely remove some undesirable regions appears in the clustering results. Therefore, these limitations will be addressed in the future work.

References:

- [1] O. Faiz, S. Blackburn, and D. Moffat, *Anatomy at a Glance*, vol. 66. John Wiley & Sons, 2011.
- [2] L. Seoud, F. Cheriet, H. Labelle, and J. Dansereau, "A novel method for the 3-d reconstruction of scoliotic ribs from frontal and lateral radiographs," *Biomedical Engineering, IEEE Transactions on*, vol. 58, no. 5, pp. 1135–1146, 2011.
- [3] N. Sverzellati, D. Colombi, G. Randi, A. Pavarani, M. Silva, S. L. Walsh, M. Pistolesi, V. Alfieri, A. Chetta, M. Vaccarezza, *et al.*, "Computed tomography measurement of rib cage morphometry in emphysema," *PloS one*, vol. 8, no. 7, p. e68546, 2013.
- [4] F. S. Gayzik, M. M. Yu, K. A. Danielson, D. E. Slice, and J. D. Stitzel, "Quantification of age-related shape change of the human rib cage through geometric morphometrics," *Journal of biomechanics*, vol. 41, no. 7, pp. 1545–1554, 2008.
- [5] F. Henry Gray, *Gray's Anatomy of the Human Body*. 1918.
- [6] K. Rathnayaka, T. Sahama, M. A. Schuetz, and B. Schmutz, "Effects of CT image segmentation methods on the accuracy of long bone 3d reconstructions," *Medical Engineering & Physics*, vol. 33, no. 2, pp. 226 – 233, 2011.
- [7] J.-Y. Zhou, D. W. Wong, F. Ding, S. K. Venkatesh, Q. Tian, Y.-Y. Qi, W. Xiong, J. J. Liu, and W.-K. Leow, "Liver tumour segmentation using contrast-enhanced multi-detector ct data: performance benchmarking of three semiautomated methods," *European radiology*, vol. 20, no. 7, pp. 1738–1748, 2010.
- [8] X. Pardo, M. Carreira, A. Mosquera, and D. Cabello, "A snake for CT image segmentation integrating region and edge information," *Image and Vision Computing*, vol. 19, no. 7, pp. 461 – 475, 2001.
- [9] R. Xu, D. Wunsch, *et al.*, "Survey of clustering algorithms," *Neural Networks, IEEE Transactions on*, vol. 16, no. 3, pp. 645–678, 2005.
- [10] R. Xu and D. C. Wunsch, "Clustering algorithms in biomedical research: a review," *Biomedical Engineering, IEEE Reviews in*, vol. 3, pp. 120–154, 2010.

- [11] H. Al-Shamlan and A. El-Zaart, "Feature extraction values for breast cancer mammography images," in *Bioinformatics and Biomedical Technology (ICBBT), 2010 International Conference on*, pp. 335–340, IEEE, 2010.
- [12] M. Nixon and A. S. Aguado, *Feature extraction & image processing*. Academic Press, 2008.
- [13] M. Mignotte, "Segmentation by fusion of histogram-based k-means clusters in different color spaces," *IEEE Transactions on image processing*, vol. 17, no. 5, pp. 780–787, 2008.
- [14] T. H. Lee, M. F. A. Fauzi, and R. Komiya, "Segmentation of CT brain images using k-means and em clustering," in *Computer Graphics, Imaging and Visualisation, 2008. CGIV'08. Fifth International Conference on*, pp. 339–344, IEEE, 2008.
- [15] L.-H. Juang and M.-N. Wu, "Mri brain lesion image detection based on color-converted k-means clustering segmentation," *Measurement*, vol. 43, pp. 941–949, 2010.
- [16] I. A. Yusoff and N. A. M. Isa, "Two-dimensional clustering algorithms for image segmentation," *WSEAS transactions on computers*, vol. 10, no. 10, pp. 332–342, 2011.
- [17] I. A. Yusoff, N. A. Mat Isa, and K. Hasikin, "Automated two-dimensional k-means clustering algorithm for unsupervised image segmentation," *Computers & Electrical Engineering*, pp. 907–917, 2013.
- [18] P. T. Selvy, V. Palanisamy, and M. Radhai, "An improved mri brain image segmentation to detect cerebrospinal fluid level using anisotropic diffused fuzzy c means," *WSEAS Transactions on Computers*, vol. 12, no. 4, pp. 145–154, 2013.
- [19] P. T. Selvy, V. Palanisamy, and M. Radhai, "A proficient clustering technique to detect csf level in mri brain images using pso algorithm," *WSEAS Transactions on Computers*, vol. 12, no. 7, pp. 298–308, 2013.
- [20] C. Chu, M. Oda, T. Kitasaka, K. Misawa, M. Fujiwara, Y. Hayashi, R. Walz, D. Rueckert, and K. Mori, "Multi-organ segmentation from 3d abdominal CT images using patient specific weighted-probabilistic atlas," in *Medical Imaging 2013: Image Processing*, pp. 86693Y–1–86693Y–7, Proc. of SPIE, 2013.
- [21] C. M. Bishop and N. M. Nasrabadi, *Pattern recognition and machine learning*, vol. 1. Springer New York, 2006.
- [22] J. C. Bezdek, R. Ehrlich, and W. Full, "Fcm: The fuzzy $i_c^j c_j^i / i_c^j$ -means clustering algorithm," *Computers & Geosciences*, vol. 10, no. 2, pp. 191–203, 1984.
- [23] M. Y. Mashor, "Improving the performance of k-means clustering algorithm to position the centers of rbf network," *International Journal of the Computer, The Internet and Management*, vol. 6, no. 2, pp. 121–124, 1998.
- [24] N. B. Smith and A. Webb, *Introduction to medical imaging: Physics, engineering and clinical applications*. Cambridge University Press, 2010.
- [25] K. Iniewski, *Medical imaging: Principles, detectors, and Electronics*. John Wiley & Sons, 2009.
- [26] W. E. Lorensen and H. E. Cline, "Marching cubes: A high resolution 3d surface construction algorithm," in *ACM Siggraph Computer Graphics*, vol. 21, pp. 163–169, ACM, 1987.
- [27] W. Narkbuakaew, H. Nagahashi, K. Aoki, and Y. Kubota, "Integration of modified k-means clustering and morphological operations for multi-organ segmentation in CT liver-images," in *Biology and Biomedical Engineering, 2014. BBE'14. International Conference on*, pp. 34–39, Europment, 2014.

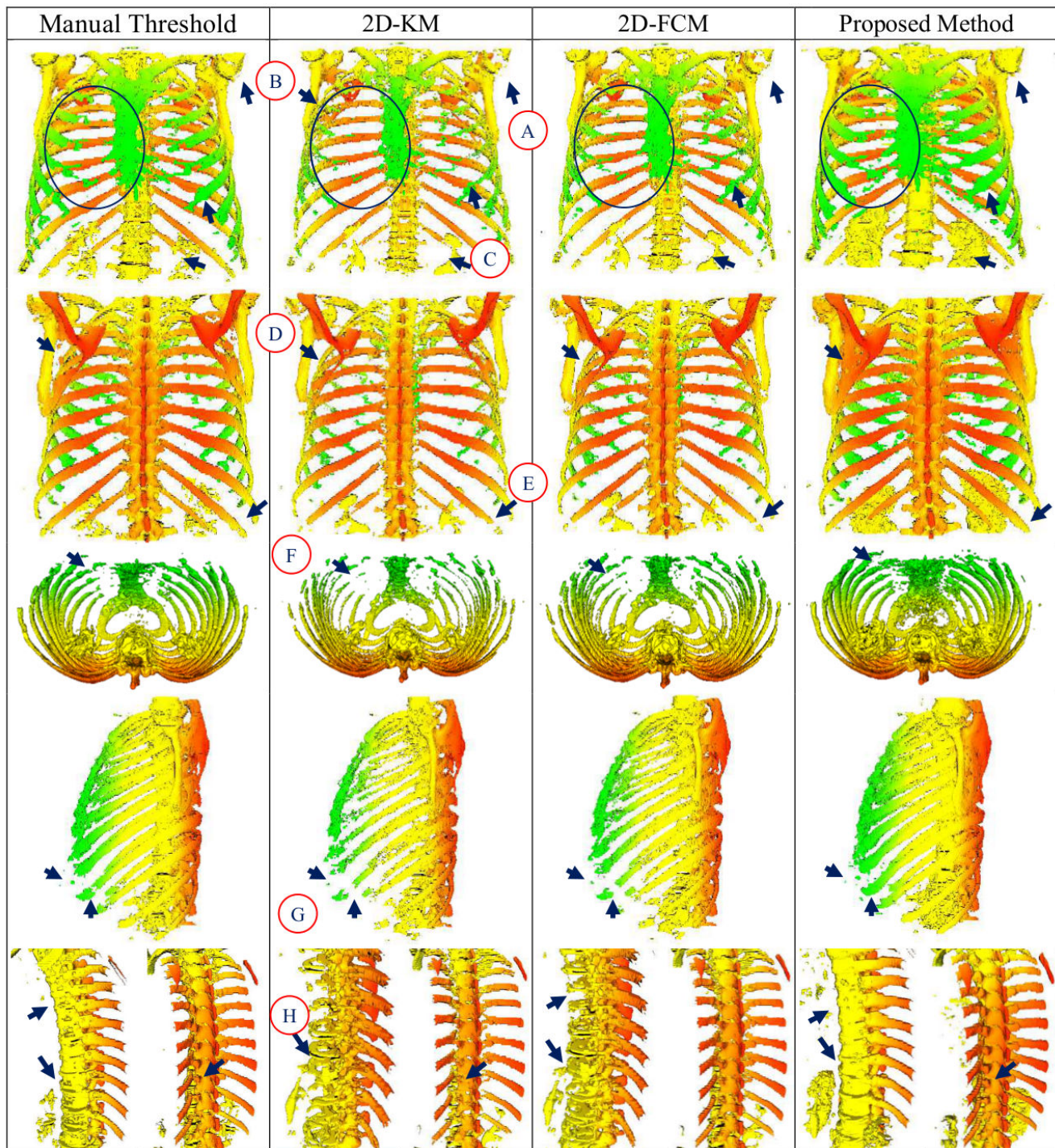


Fig. 10: Examples of 3D rib cage surface-models reconstructed from binary images, which are results of manual threshold, 2D-KM, 2D-FCM, and the proposed method. The 1st to 4th rows present front, back, bottom, and side views. The last row represent enlargement of some parts of spine.